

The Effects of Orbital Environment on X-ray CCD Performance

Catherine E. Grant, Beverly LaMarr, Eric D. Miller, and Marshall W. Bautz

Kavli Institute for Astrophysics and Space Research, Massachusetts Institute of Technology, Cambridge, MA 02139, USA e-mail: cgrant@space.mit.edu

ABSTRACT

Context. The performance of CCD detectors aboard orbiting X-ray observatories slowly degrades due to accumulating radiation damage.

Aims. In an effort to understand the relationship between CCD spectral resolution, radiation damage, and the on-orbit particle background, we attempt to identify differences arising in the performance of two CCD-based instruments: the Advanced CCD Imaging Spectrometer (ACIS) aboard the Chandra X-ray Observatory, and the X-ray Imaging Spectrometer (XIS) aboard the Suzaku X-ray Observatory.

Methods. We compare the performance evolution of front- and back-illuminated CCDs with one another and with that of very similar detectors installed in the ACIS instrument aboard *Chandra*, which is in a much higher orbit than *Suzaku*. We identify effects of the differing radiation environments as well as those arising from structural differences between the two types of detector.

Results. There are some differences and these are they.

Key words. some keywords

1. Introduction

Charged-coupled devices (CCDs) as astronomical X-ray detectors have become nearly ubiquitous since their first use in sounding rocket flights in the late 1980s. CCDs provide excellent quantum efficiency with moderate spectral resolution over a broad energy range (~ 0.1 – 10 keV) and are well-suited as imaging spectrometers as well as readout detectors for dispersive gratings. Currently, CCDs are focal plane detectors in five operating X-ray observatories from NASA, ESA and JAXA, and are planned to be part of many upcoming missions.

Radiation damage is a common concern in all spacecraft components. One symptom of radiation damage in CCDs is an increase in the number of charge traps (?) **Ref TBA**. When charge is transferred across the CCD to the readout, some portion can be captured by the traps and gradually re-emitted. If the original charge packet has been transferred away before the traps re-emit, the captured charge is “lost” to the charge packet. This process is quantified as charge transfer inefficiency (CTI), the fractional charge loss per pixel. As a result, the amount of charge (or the pulseheight) read out from the instrument decreases with increasing transfer distance; since this pulseheight corresponds directly to the incoming X-ray photon energy, the measured energy also decreases. In addition, the spectral resolution degrades due to noise in the charge trapping and re-emission process, non-uniform trap distribution, and variations in trap occupancy. All of these processes apply to the charge in each pixel, so multi-pixel X-ray events will be more degraded than single-pixel events.

Measured CTI is a function of fluence, or, more specifically, the amount of charge deposited on the CCD. As the fluence increases, traps filled by one charge packet may remain filled as a second charge packet is transferred through the pixel. The second charge packet sees fewer unoccupied traps as a result of the previous “sacrificial charge” and loses less charge than it would have otherwise (Gendreau et al. 1993). This sacrificial charge

can be in the form of X-rays, charged particle interactions, or intentionally injected charge.

The response of a CCD-based instrument is thus partially determined by its particle environment, whether causing radiation damage or providing sacrificial charge, which in turn is dependent on the spacecraft orbit. The Advanced CCD Imaging Spectrometer (ACIS) on the *Chandra X-ray Observatory* (Weisskopf et al. 2002) and the X-ray Imaging Spectrometer (XIS) on the *Suzaku X-ray Observatory* (Mitsuda et al. 2007) utilize similar CCDs but occupy very different radiation environments. The two instruments combined have produced more than eighteen years worth of monitoring data which provides a unique opportunity to better understand the relationship between X-ray CCD spectral resolution, radiation damage, and the on-orbit particle background.

We begin by describing the differences and similarities of the instruments, spacecraft orbits, and on-board calibration sources in Section 2. Section 3 outlines our data analysis procedures while Section 4 discusses the results.

2. Description of the Instruments

2.1. CCD Detector Characteristics

The CCD chips in ACIS and the XIS were fabricated at MIT Lincoln Laboratory and are very similar in design. The ACIS CCDs predate the XIS CCDs by nearly a decade so some small differences do exist.

Chandra has a single X-ray telescope and a moveable Science Instrument Module (SIM), which can move ACIS in and out of the telescope focus. The ACIS focal plane consists of ten CCD devices (MIT Lincoln Laboratory CCD17), eight of which are front-illuminated (FI) and two of which are back-illuminated (BI). The layout of the ACIS devices is shown in Figure 1. The CCD characteristics are summarized in Table 1 and described in detail by Garmire et al. (2003).

Suzaku has four XIS instruments, each with an independent X-ray Telescope (XRT) and focal plane assembly. The four devices are model CCID41, comprising three FI chips (XIS0, XIS2, and XIS3) and one BI (XIS1). The layout of the XIS devices is shown in Figure 2. One of the FI devices (XIS2) was damaged by a likely micrometeorite strike in October 2006 and has been unused since that time. The CCDs are summarized in Table 1 and described in detail by Koyama et al. (2007). The XIS devices are physically very similar to the ACIS devices with one notable exception, the addition of charge injection capabilities in the XIS CCID41 (Bautz et al. 2007). This allows a controlled amount of charge to be injected from a register at the top of the array into individual pixels, rows, or a variety of patterns as the CCD is clocked. The injected charge is read out along with the other charge packets in the array.

While the CCDs are reasonably similar, there are a number of important operational differences. The individual frame exposure time for XIS is more than twice as long as for ACIS. Given the same particle or X-ray flux, the longer frame time of XIS will yield more sacrificial charge than seen on ACIS. Another important difference is the operating temperature of the detector. ACIS is kept much colder than XIS, which reduces incidence of warm pixels. Depending on the characteristics of the electron traps, the temperature can also change the measured CTI. In the case of the ACIS BI CCDs, the initial CTI is all due to damage during manufacturing, and the performance is slightly better at warmer temperatures. The CTI of the ACIS FI CCDs is entirely due to radiation damage, so the CCDs are highly sensitive to temperature and have much lower CTI at -120°C (Grant et al. 2006). Similarly, the row-to-row transfer times are slightly different which, depending on the time constants of the electron traps, can change the measured CTI.

Finally, charge injection, while initially turned off for the XIS detectors, has been the standard operating mode since November 2006 (Uchiyama et al. 2009). In this mode a full row of charge equivalent to 6 keV for the FI chips (2 keV for the BI chip) is injected every 54 rows, or every 1.3 ms during the chip read out. The level of injected charge was increased to 6 keV for the BI chip in June 2011, however we exclude those observations from the analysis presented here.

As already noted above, between the time that ACIS and XIS were built, some improvements were made in the BI manufacturing process. The ACIS BI CCDs had measurable CTI across the entire array, including the framestore and serial readout array, from defects induced in during the manufacturing process. The performance of the XIS BI CCD was nearly the same as the FI CCDs pre-launch, due to an improved manufacturing process further described in Burke et al. (2004) and Bautz et al. (2004).

For the purposes of this paper, we are only examining parallel CTI, or charge loss as a function of row number. Serial CTI, charge loss as a function of columns, is negligible for both XIS and ACIS except in the case of the ACIS BI CCDs, and even then it is not evolving on orbit.

2.2. Orbital Radiation Environments

ACIS and XIS occupy quite different radiation environments. *Chandra* is in a highly elliptical, 2.7-day orbit that transits a wide range of particle environments, from the Earth's radiation belts at closest approach through the magnetosphere and magnetopause and past the bow shock into the solar wind (O'Dell et al. 2000). Soon after launch it was discovered that the FI CCDs had suffered radiation damage from exposure to soft protons (~ 0.1 – 0.5 MeV) scattered off *Chandra's* grazing-incidence optics dur-

ing passages through the radiation belts (Prigozhin et al. 2000). The BI CCDs were unaffected due to the much deeper buried channel. Since the discovery of the radiation damage, ACIS has been protected during radiation belt passages by moving it out of the focal plane. Radiation damage to the CCDs has continued at a much slower rate, due to soft protons scattered by the optics during observations, and strongly penetrating solar protons and cosmic rays which pass through the spacecraft shielding. The particle background on the detector consists of a quiescent portion that is anti-correlated with the solar cycle, and soft proton flares (Grant et al. 2002).

Suzaku is in a 96-minute, low-Earth orbit with an inclination of 32 degrees and gains some protection from cosmic rays by the Earth's geomagnetic field (Mitsuda et al. 2007). Many orbits pass through the South Atlantic Anomaly (SAA), a region of enhanced particle flux, which requires the instruments to be shut off. The particle background on the XIS detectors is produced by cosmic rays that penetrate the spacecraft shielding (Mizuno et al. 2004); it is generally lower for XIS than for ACIS and varies throughout the orbit as a function of the geomagnetic cut-off rigidity, a measure of how well the Earth's geomagnetic field shields the spacecraft from charged particles (Tawa et al. 2008).

2.3. Calibration Sources

Both ACIS and XIS have on-board radioactive ^{55}Fe sources used for instrument monitoring and calibration. The ACIS External Calibration Source (ECS) is mounted such that it is only viewable when ACIS is moved out of the focal plane. Observations of the ECS are done twice an orbit, just before and after perigee. The ECS provides roughly uniform illumination of the entire focal plane. Fluorescent Al and Ti targets provide lines at 1.5 keV (Al K) and 4.5 keV (Ti K α), as well as those from the ^{55}Fe source itself at ~ 0.7 keV (Mn L), 5.9 keV (Mn K α), and 6.4 keV (Mn K β).

The calibration sources on XIS illuminate the upper corners of each CCD during all observations. The spectral lines are from the ^{55}Fe source itself at 5.9 keV (Mn K α) and 6.4 keV (Mn K β). The orientation and approximate size of the regions illuminated by the calibration sources are shown in Figure 2.

3. Methodology

3.1. Data and Analysis

The data used here have not gone through the standard pipeline processing that is normally applied to data distributed to users. Standard processing¹ is designed to remove some of the effects we are trying to study here, by applying corrections for CTI and time-dependent gain changes. The actual performance seen by a typical user from standard pipeline processed data is much improved from that seen here. The data have been minimally processed, by removing the CCD bias level and by applying a standard grade filter (ASCA G02346) and discard all others. XIS1 and ACIS-S3 are used as representative BI CCDs and XIS3 and ACIS-I3 are representative FI CCDs.

As the XIS calibration sources only illuminate the upper corners of the CCDs, we filter the data to include only events within a rectangular region encompassing the calibration source events. The size of the region varies slightly between CCDs, but is roughly 225 pixels square. While the ACIS calibration sources

¹ See <http://cxc.harvard.edu/ciao/threads/data.html> and <http://heasarc.gsfc.nasa.gov/docs/suzaku/analysis/abc/>

fully illuminate the CCDs, the data were also filtered to roughly match the XIS regions.

The individual calibration source observations are then grouped together by time in bins of roughly a month. The ACIS data cover the time period from January 2000, when the focal plane temperature was initially lowered to its current value, to February 2011. The XIS data begin shortly after the *Suzaku* launch in July 2005 and continue through February 2011. The XIS data with and without charge injection are binned separately, as the performance is quite different.

The gain of the detector, the transformation from pulseheight to energy for each event, is determined by fitting a Gaussian to the pulseheight histogram in the initial time bin. The two corner regions must be fit separately, since they are in different readout nodes and do not have the same gain. This gain correction is then applied to all the time bins.

We then make an energy spectrum of the data in each time bin. Since we have already applied a gain correction, the two corner regions can now be combined into one spectrum and fit together. A Gaussian plus a linear background term is fit to the region around the Mn $K\alpha$ line. The Gaussian centroid and width are used in the subsequent sections to understand the evolution of CTI.

3.2. A Proxy for Measuring CTI

A standard measurement of parallel CTI, or charge loss as a function of row, requires full illumination of the CCD with a source of known energy. The ECS on ACIS is capable of illuminating the entire CCD array with photons at a number of specific energies, as described in Section 2.3. The CTI on XIS is calibrated in a number of less direct ways, including a novel method of “checker flag” charge injection described further in Ozawa et al. (2009). Since the XIS calibration sources are incapable of illuminating the full chip, for proper comparison we must restrict our analysis to the upper corners of the ACIS chips as well. A change in CTI must change the accumulated charge loss and thus the pulseheight far from the framestore region. A change in pulseheight, however, does not necessarily have to be related to CTI; it could also be due to changes in the gain completely unrelated to radiation damage. For example, ACIS has a known slow change in the gain as a function of time as measured very close to the framestore where CTI should be negligible. For most of the CCDs it is monotonically decreasing at a rate of ~ 1 ADU yr^{-1} at 5.9 keV.²

To determine the feasibility of using only the upper corners as a CTI metric, we compared the change in Mn $K\alpha$ pulseheight to the measured CTI for two ACIS chips. The results are shown in Figure 3. Prior to correcting for the known gain change, the fractional pulseheight change is well-correlated to the CTI (left panels). After the correction, the correlation is even tighter (right panels). The correction coefficient was fit by eye, finding the value **the** best reduced the ACIS-I3 scatter. The correction is always less than 0.5% of the total pulseheight.

While the electronics of the two instruments are not identical, there’s no reason to assume the relationship of the line centroid to CTI would be any different for XIS than for ACIS.

(maybe Bev/Eric can add something more? XIS gain evolution must be monitored by sky sources, which should indicate if there’s lots of non-CTI gain change going on) should

² See <http://space.mit.edu/home/cgrant/gain> for example plots of the gain change.

also be more specific electronic gain changes versus framestore CTI changes

4. Discussion

4.1. CTI Time Evolution

The time evolution of CTI, as measured by the change in the line energy, is shown in Figures 4 and 5 for XIS and ACIS, respectively. The change in line energy is plotted as the fractional change since the first data point. Data from both front- and back-illuminated devices are included, as well as both with and without XIS charge injection.

Increasing CTI leads to decreasing measured line energy. All cases show an overall increase in CTI due to radiation damage. In some cases, the CTI increase from radiation damage is modified by sacrificial charge from the particle background, discussed further in Section 4.3. Charge injection also clearly modifies the rate of CTI increase. The rate of change of CTI varies substantially between the different cases.

4.1.1. Suzaku

Figure 4 shows the change in line energy for XIS. Initially, charge injection was not used, so the early data is all with charge injection turned off. The rate of line energy change is roughly 2% per year without charge injection and the FI and BI devices, while not identical, appear very similar. The line energy evolution appears to be approximately linear with time.

When charge injection is turned on, there are three obvious changes. The first is that the line energy jumps up, since the charge injection produces significant sacrificial charge which improves the measured CTI. The second is that the rate of change of line energy is shallower than without charge injection. Finally, the improvement due to charge injection is larger for the FI CCD than for the BI device. The rate of line energy change is roughly 1% per year for the BI CCD and 0.4% per year for the FI CCD. The FI/BI difference is due to the fact that the amount of charge injected is three times higher on the FI CCDs than the BI CCDs (Bautz et al. 2007).

4.1.2. Chandra

Figure 5 shows the change in line energy for ACIS. ACIS does not have the capability to inject a known quantity of charge like XIS, so the only sacrificial charge is from the particle background and the X-ray photons themselves. This is clearly seen in the structure of the line energy as a function of time which contains distinct features that are also found in the particle background (Figure 11).

The rate of line energy change is much lower for ACIS than it is for XIS. Assuming a linear decay, the change is roughly 0.1% per year for the BI CCD and 0.07% per year for the FI CCD. The decrease is clearly not strictly linear, due to the changing sacrificial charge which adds both features from individual solar storms and a larger modification tied to the solar cycle.

The evolution of the FI and BI CCDs look quite different as well. The FI CCDs appear to be much more sensitive to sacrificial charge from the particle background than the BI CCDs. This cannot be due to differences in the number and type of particles impinging on the CCDs, but in how the particles interact with the CCD structure. Sacrificial charge from the changing particle background and the FI/BI difference will be discussed further in Section 4.3.

4.2. Spectral Resolution Time Evolution

The time evolution of spectral resolution is shown in Figures 6 and 7 for XIS and ACIS, respectively. The spectral resolution is measured as the FWHM of the Mn $K\alpha$ line. Data from both front- and back-illuminated devices are included, as well as both with and without XIS charge injection.

The relationship between increasing CTI and spectral resolution is not as simple as that for line energy. If an X-ray event occupies a single pixel, the charge loss due to CTI essentially adds an additional noise term to the spectral resolution. In the case of both ACIS and XIS, many events are split over multiple pixels. In that case, charge loss adds additional noise terms from all of the split pixels. In addition, some of the lost charge may be re-emitted into a trailing pixel which may also be included in the event depending on the size of the trailing charge.

4.2.1. Suzaku

Figure 6 shows the change in spectral resolution as a function of time for XIS. Initially, before charge injection was turned on, the rate of increase of spectral resolution for FI and BI CCDs was very similar, about 70 eV per year. Once charge injection was turned on, the performance improved and FWHM dropped to nearly the initial value. The rate of increase is much slower with charge injection than without, although again, the FI CCD shows more improvement than the BI CCD due to the smaller amount of injected charge. The FWHM increase is about 12 eV per year for the FI CCD and about 28 eV per year for the BI CCD.

4.2.2. Chandra

Figure 7 shows the change in spectral resolution as a function of time for ACIS. The initial FWHM for both ACIS devices is much higher than that for XIS. This is due to the pre-launch manufacturing defects on the BI CCD and the initial radiation damage to the FI CCDs in 1999, before the time period shown here. The rate of increase, however, is vanishingly small, less than 1 eV per year for the BI CCD and consistent with no change for the FI CCD. Unlike the line energy, the FWHM evolution shows no obvious dependence on the particle background.

4.3. CTI and Spectral Resolution: Dependence on Background

As stated previously, measured CTI is a function of the amount of charge deposited on the CCD. Figure 8 shows images of typical raw CCD frames for both ACIS and XIS and both types of CCDs. Essentially all the visible features are due to cosmic ray charged particles. While the images do include X-ray events from the calibration sources, they are nearly invisible due to their small size and low numbers.

The most obvious difference is that between the FI and BI CCDs due to their structural differences. The FI CCDs display large streaks and blobs while the BI CCDs have much smaller features. The FI CCDs have an active, depleted region and a much thicker field-free region. The X-ray events generally interact in the depleted region so the charge is collected in a small area. Charge particles can traverse the entire thickness of the CCD, depositing charge along their path. The charge in the field-free region can disperse more freely and produces the large blobs seen in the image. The BI CCDs are fully depleted, without the additional field-free region. The charge from particles stays

more concentrated into smaller blobs and streaks. Comparing the FI and BI images from a single instrument, such as ACIS, shows that the total number of particle events is comparable even though their morphology is so different.

The number of particle events is also different between XIS and ACIS. ACIS clearly shows more particle events than XIS, even though the ACIS frame exposure time, 3.2 sec, is less than half that of XIS, 8 sec. This is due to the particle environment in the two orbits. Suzaku is in a low-earth orbit and receives substantial shielding from the Earth's magnetic field while Chandra's orbit takes it well above the magnetosphere and does not receive the same shielding. One might assume that the higher particle rate on the ACIS raw frames would translate to faster accumulation of radiation damage that is not seen in the comparison between Figures 4 and 5.

These basic differences in the number and morphology of particle events can explain some of the differences between the CTI evolution of ACIS and XIS. An additional piece of the puzzle is the time-dependence of the particle events themselves. Figure 11 shows a measure of the ACIS particle background over the same time period and with the same binning as the CTI evolution data. In this case the rate of high energy events rejected on-board the spacecraft is used as a proxy for the particle background rate. These events are well above the X-ray energies that can be focused by the telescope and can only be caused by particles. The particle background rate is clearly not constant but is at the lowest level in 2001 and reaches more than twice that level in 2010. It has been shown that this measure of the ACIS particle background is well correlated over long time-scales with proton fluxes measured by the ACE spacecraft with energies above 10 MeV (Grant et al. 2002). The lower particle fluxes are due to extra shielding provided by the solar magnetic field during solar maximum. Additional smaller scale dips can be seen which can be directly linked to increased heliomagnetic shielding during specific solar storms. The solar storms also produce transient increases in the particle background, but these are over much shorter timescales, hours to days, and thus do not appear in Figure 11.

CTI and therefore peak are well known to correlate to background (ref here), higher background provides more sacrificial charge and thus lower CTI higher peak. is fwhm also correlated? yes, very weakly

Due to the shielding from the Earth's magnetic field, the long-term variability of the XIS particle background is very small. Tawa et al. (2008) found that after removing the orbital modulation and with the exception of a brief period of high solar activity, the particle background on XIS was constant within $\pm 6\%$ per year. A much stronger variability is induced by the Earth's geomagnetic field as the spacecraft travels about its ~ 96 -minute orbit.

Figures 9 and 10, XIS peak and fwhm vs COR.

4.4. CTI and Spectral Resolution: Dependence on Temperature

At least some of the differences between the evolution of CTI on ACIS and XIS can possibly be due to operating at different focal plane temperatures. ACIS is much colder at -120°C than XIS at -90°C , so many of the common electron traps that cause CTI have been frozen out. In particular, the rate of change of CTI is much higher on XIS than ACIS. While this could be due to a higher level of damaging particle radiation, it could also be due to the higher CCD temperatures.

The ACIS team has performed a series of CTI measurements at different temperatures at two different times (Grant et al. 2006). By comparing the time evolution at -120°C and -90°C we can determine how large the CTI change on ACIS would be at either temperature.

5. Conclusions

Acknowledgements. The authors thank blah blah and blah blah for such and such. This work was supported by NASA grant so and so.

References

- Bautz, M. W., Kissel, S. E., Prigozhin, G. Y., et al. 2004, in Society of Photo-Optical Instrumentation Engineers (SPIE) Conference Series, Vol. 5501, Society of Photo-Optical Instrumentation Engineers (SPIE) Conference Series, ed. A. D. Holland, 111–122
- Bautz, M. W., LaMarr, B. J., Miller, E. D., et al. 2007, in Society of Photo-Optical Instrumentation Engineers (SPIE) Conference Series, Vol. 6686, Society of Photo-Optical Instrumentation Engineers (SPIE) Conference Series
- Burke, B. E., Gregory, J. A., Loomis, A. H., et al. 2004, IEEE Transactions on Nuclear Science, 51, 2322
- Garmire, G. P., Bautz, M. W., Ford, P. G., Nousek, J. A., & Ricker, Jr., G. R. 2003, in Society of Photo-Optical Instrumentation Engineers (SPIE) Conference Series, Vol. 4851, Society of Photo-Optical Instrumentation Engineers (SPIE) Conference Series, ed. J. E. Truemper & H. D. Tananbaum, 28–44
- Gendreau, K., Bautz, M., & Ricker, G. 1993, Nuclear Instruments and Methods in Physics Research A, 335, 318
- Grant, C. E., Bautz, M. W., Kissel, S. E., LaMarr, B., & Prigozhin, G. Y. 2006, in Society of Photo-Optical Instrumentation Engineers (SPIE) Conference Series, Vol. 6276, Society of Photo-Optical Instrumentation Engineers (SPIE) Conference Series
- Grant, C. E., Bautz, M. W., & Virani, S. N. 2002, in Astronomical Society of the Pacific Conference Series, Vol. 262, The High Energy Universe at Sharp Focus: Chandra Science, ed. E. M. Schlegel & S. D. Vrtilek, 401
- Koyama, K., Tsunemi, H., Dotani, T., et al. 2007, PASJ, 59, 23
- Mitsuda, K., Bautz, M., Inoue, H., et al. 2007, PASJ, 59, 1
- Mizuno, T., Kamae, T., Godfrey, G., et al. 2004, ApJ, 614, 1113
- O'Dell, S. L., Bautz, M. W., Blackwell, W. C., et al. 2000, in Society of Photo-Optical Instrumentation Engineers (SPIE) Conference Series, Vol. 4140, Society of Photo-Optical Instrumentation Engineers (SPIE) Conference Series, ed. K. A. Flanagan & O. H. Siegmund, 99–110
- Ozawa, M., Uchiyama, H., Matsumoto, H., et al. 2009, PASJ, 61, 1
- Prigozhin, G. Y., Kissel, S. E., Bautz, M. W., et al. 2000, in Society of Photo-Optical Instrumentation Engineers (SPIE) Conference Series, Vol. 4140, Society of Photo-Optical Instrumentation Engineers (SPIE) Conference Series, ed. K. A. Flanagan & O. H. Siegmund, 123–134
- Tawa, N., Hayashida, K., Nagai, M., et al. 2008, PASJ, 60, 11
- Uchiyama, H., Ozawa, M., Matsumoto, H., et al. 2009, PASJ, 61, 9
- Weisskopf, M. C., Brinkman, B., Canizares, C., et al. 2002, PASP, 114, 1

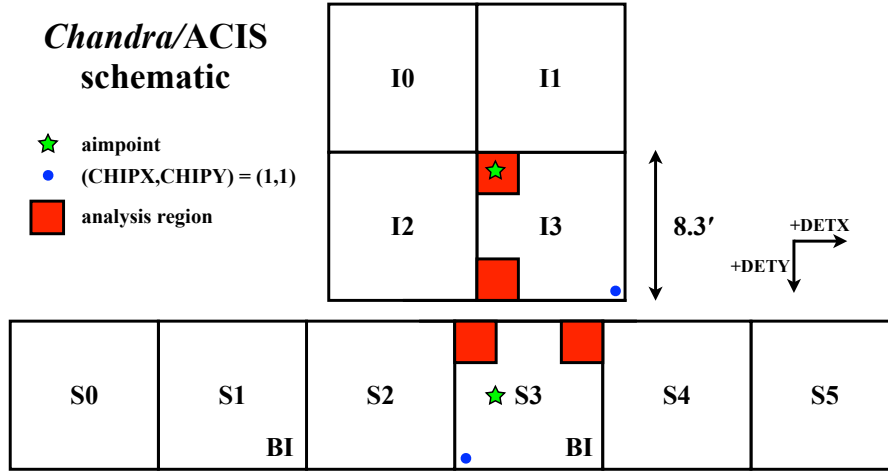


Fig. 1. Schematic drawing of the ACIS focal plane. The orange squares indicate the regions used for data analysis in this paper. The green stars show the standard aimpoints on ACIS-I3 and ACIS-S3.

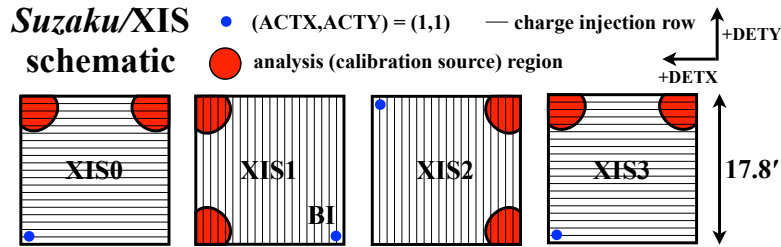


Fig. 2. Schematic drawing of the XIS focal plane. The orange circles show the regions illuminated by the ^{55}Fe sources. The light grey lines indicate the direction and spacing of the charge injection rows.

Table 1. Characteristics of MIT Lincoln Laboratory CCDs for ACIS and XIS

	ACIS	XIS
Model	CCID17	CCID41
Format	1026 rows \times 1024 pixels/row (imaging area)	
Architecture	3-phase, frame-transfer, four parallel output nodes	
Illumination Geometry	8 FI & 2 BI	2 FI & 1 BI
Charge Injection Capable	no	yes
Pixel Size	$24 \times 24 \mu\text{m}$	
Readout Noise (RMS)	$2\text{--}3 \text{ e}^-$ at 400 kpix s^{-1}	$< 2.5 \text{ e}^-$ at 41 kpix s^{-1}
Depletion Depth	FI: $64\text{--}76 \mu\text{m}$; BI: $30\text{--}40 \mu\text{m}$	FI: $60\text{--}65 \mu\text{m}$; BI: $40\text{--}45 \mu\text{m}$
Operating Temperature	-120°C via radiative cooling	-90°C via Peltier cooler
Frame Transfer Time (per row)	$40 \mu\text{s}$	$24 \mu\text{s}$
Frame Exposure Time ^a	3.2 s	8.0 s
Pre-Launch CTI (10^{-5})	FI: < 0.3 BI: 1–3	FI: 0.3–0.5 BI: 0.55

^(a) In normal operating mode.

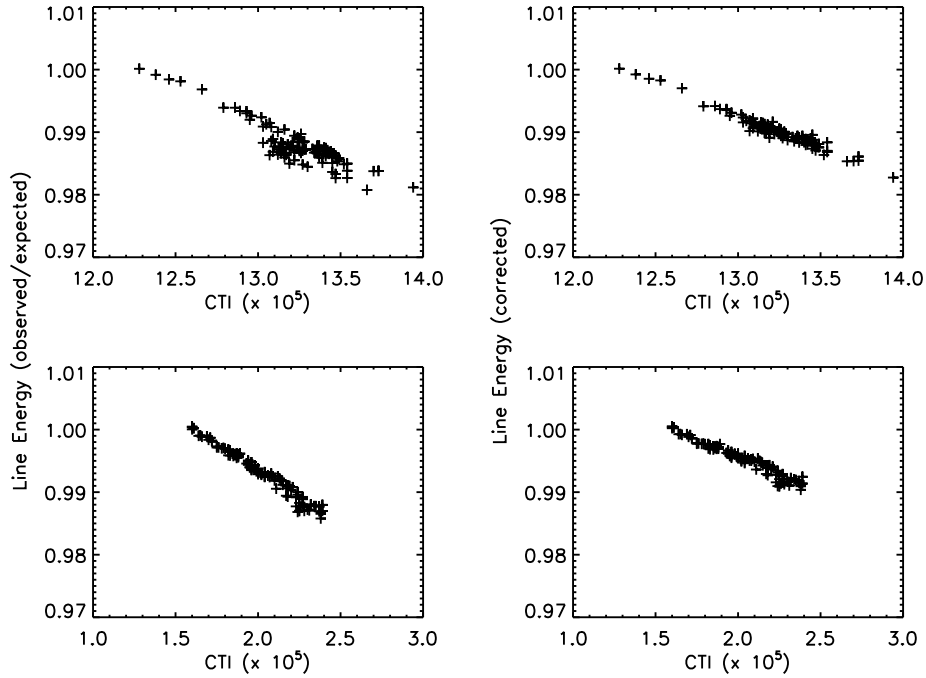


Fig. 3. CTI ($\times 10^5$) versus the fractional change in Mn $K\alpha$ line energy for two ACIS devices, the FI CCD I3 (top) and the BI CCD S3 (bottom), as measured from the upper corners of each chip. The left panels show the measured data, while the right panels show data corrected for a slow gain decrease, discussed in the text. The CTI and pulseheight are well-correlated.

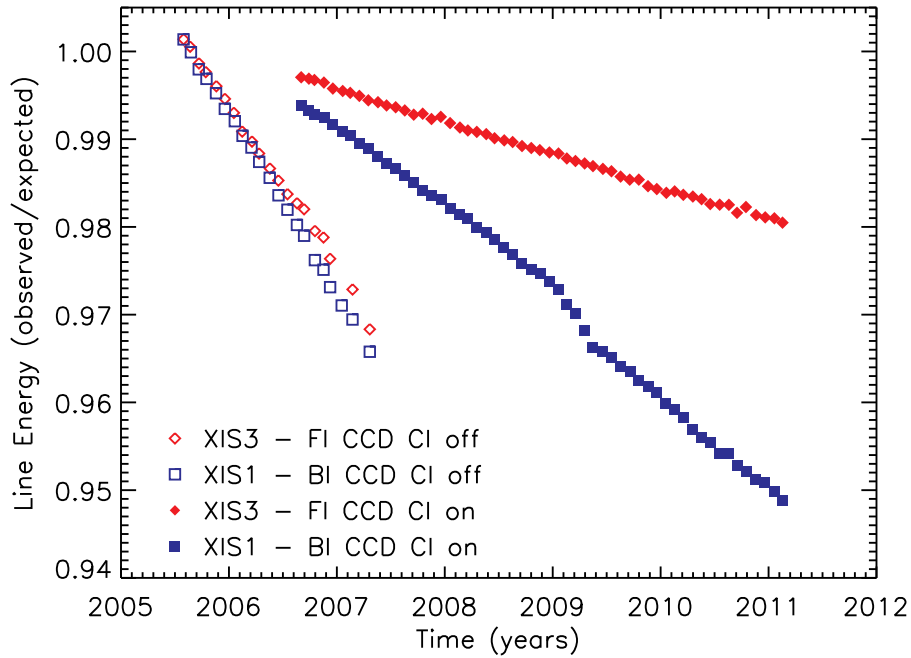


Fig. 4. Fractional change in the measured XIS central line energy over the course of the *Suzaku* mission, as measured at Mn $K\alpha$. Different symbols show FI and BI devices with charge injection (CI) on and off.

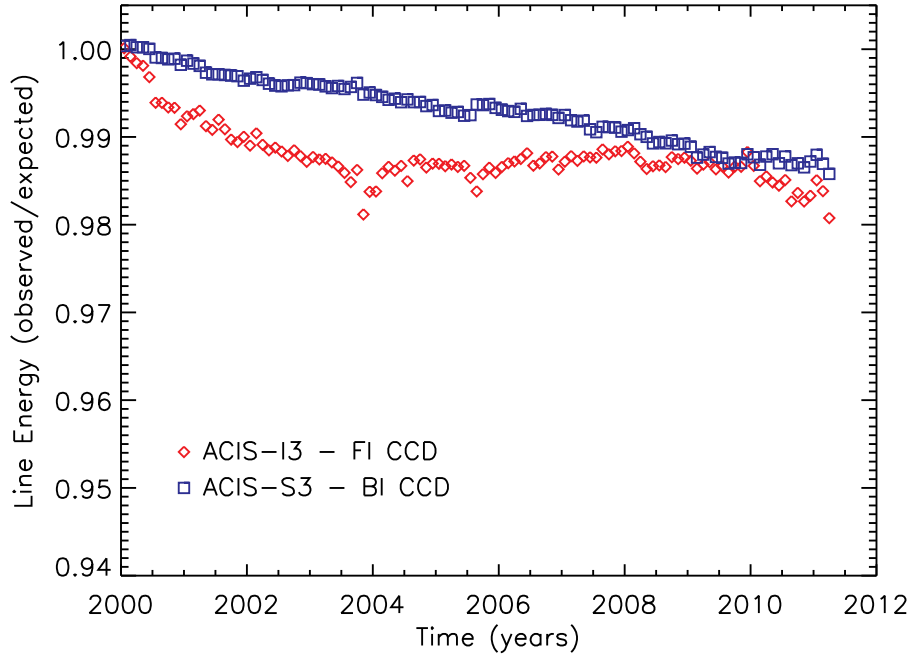


Fig. 5. Fractional change in ACIS line central energy over the course of the *Chandra* mission, as measured at Mn $K\alpha$. The effects of varying particle background and sacrificial charge are seen in the ACIS-I3 (FI) data.

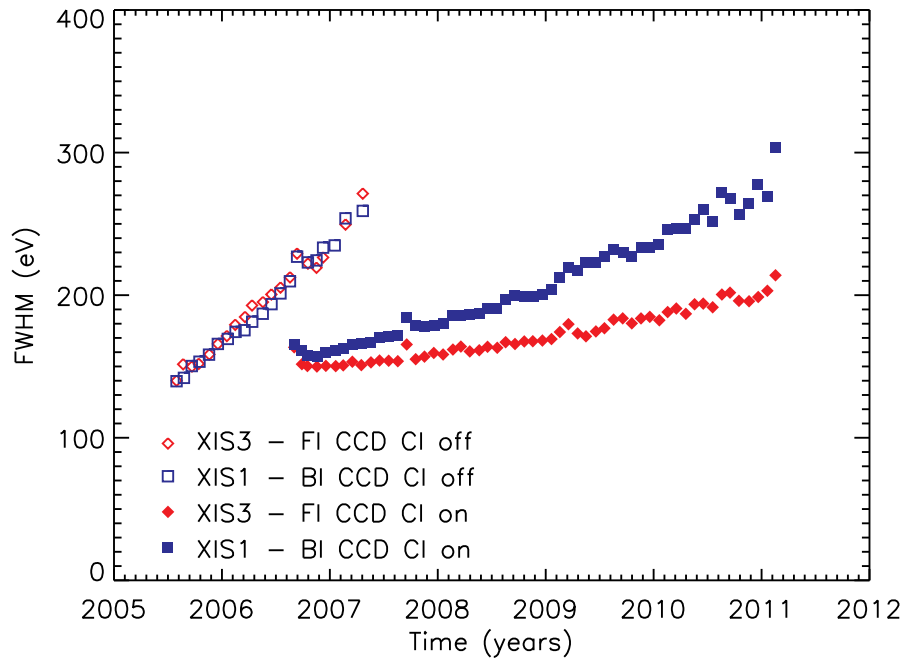


Fig. 6. Change in XIS line width (FWHM) with time over the course of the *Suzaku* mission, as measured at Mn $K\alpha$. Different symbols show FI and BI devices with charge injection (CI) on and off.

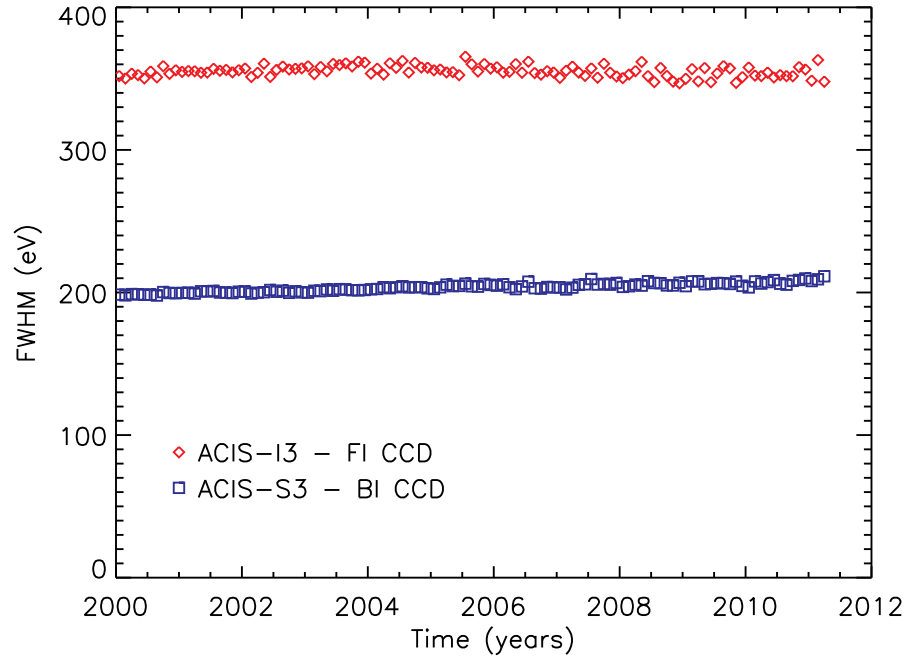


Fig. 7. Change in ACIS line width over the course of the *Chandra* mission, as measured at Mn $K\alpha$.

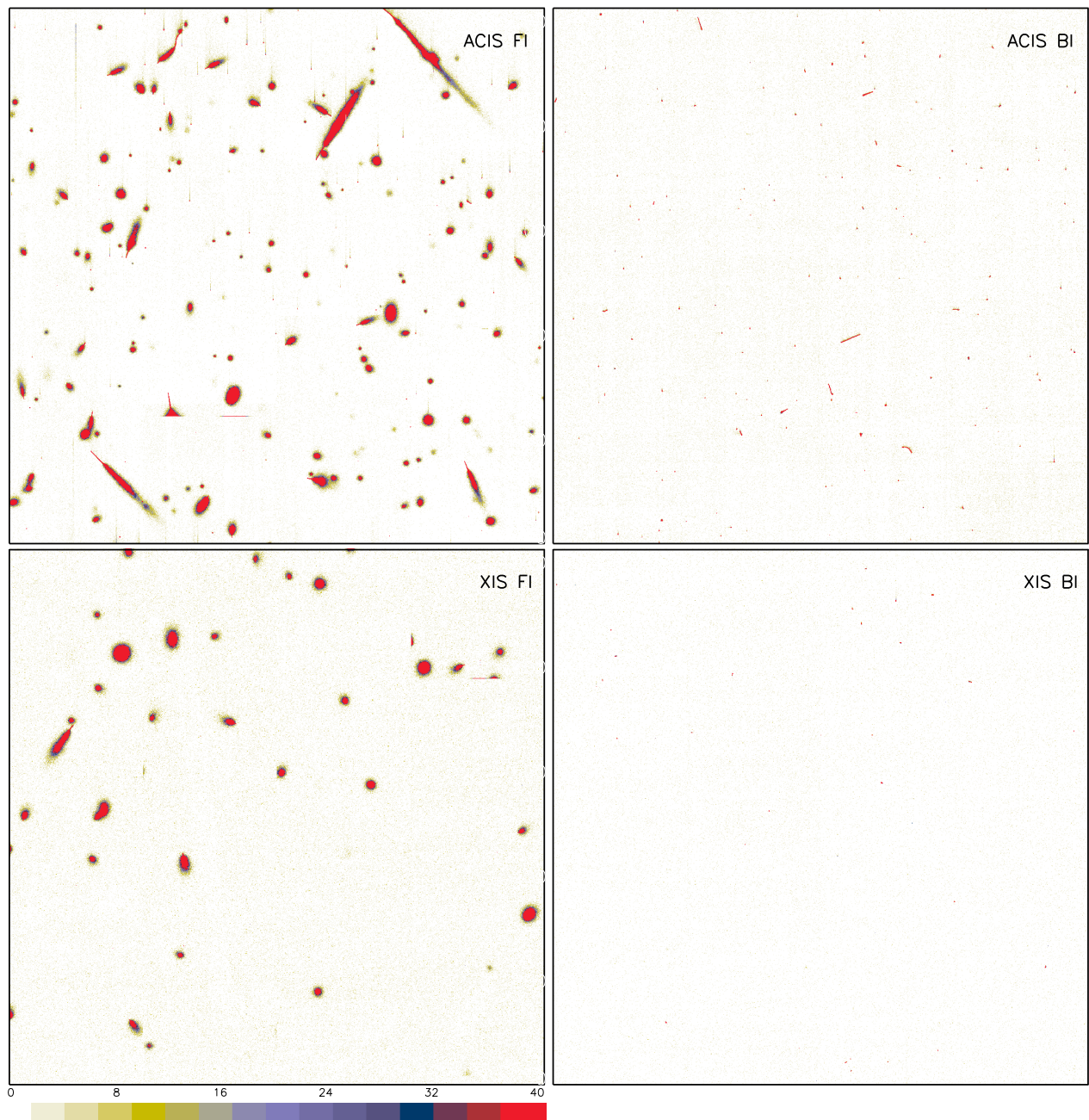


Fig. 8. Raw frame images for ACIS (top) and XIS (bottom), showing an FI (left) and BI (right) device for each. The colorbar shows the pixel values in ADU. An X-ray event from ^{55}Fe would have a pulseheight around 1500 ADU. The differences between the FI and BI CCDs, and between ACIS and XIS are explained in the text.

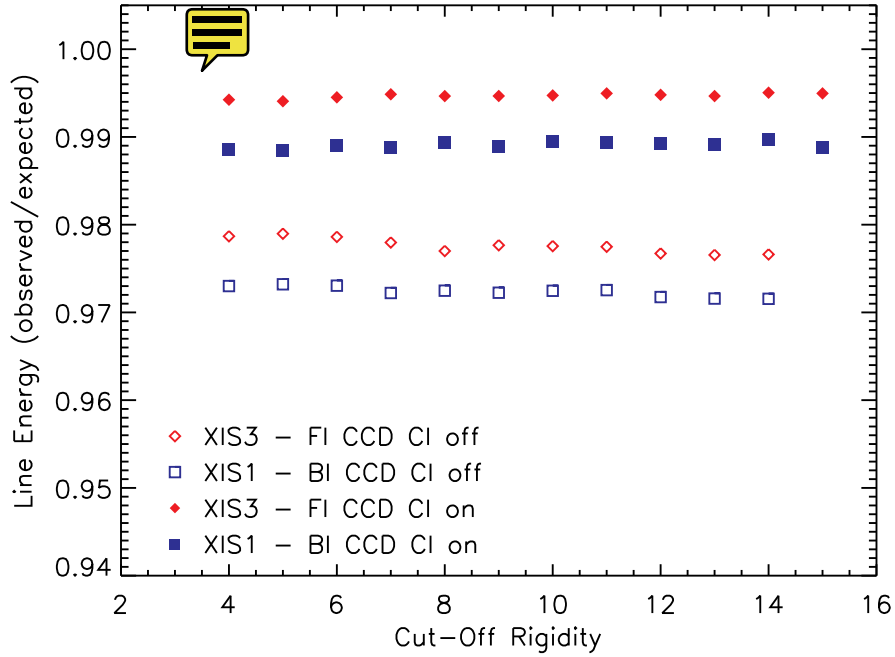


Fig. 9. Fractional change in the XIS line energy as a function of COR, averaging over October–November 2006. Symbols are the same as in Figure 4. A trend toward lower line energy (increased CTI) with higher COR (decreased background) is seen in the FI, charge injection (CI) off data. This results from lower amounts of sacrificial charge. As with the line width in Figure 10, use of charge injection overwhelms the effects of sacrificial charge (solid points).

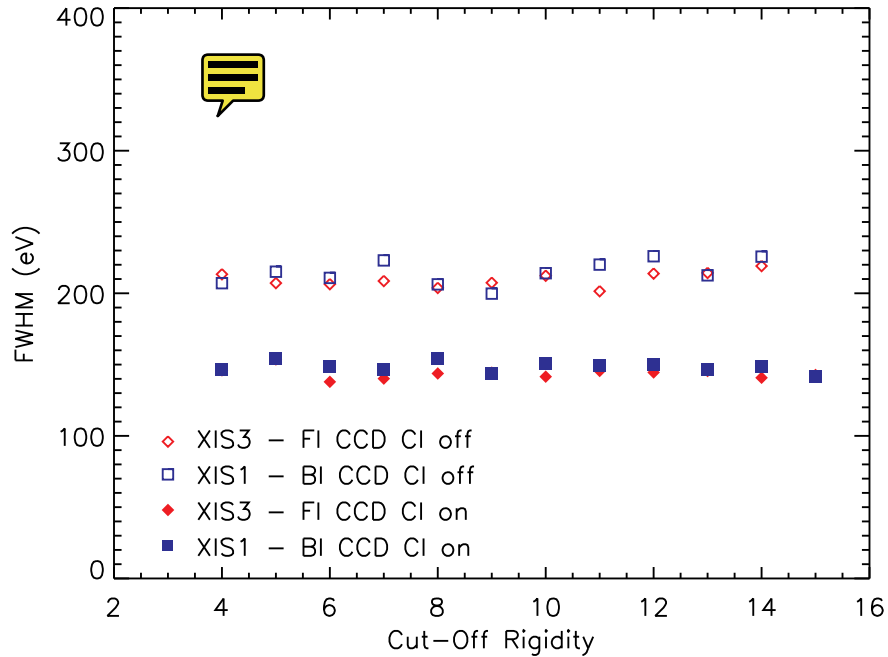


Fig. 10. XIS Mn $K\alpha$ line width (FWHM) as a function of the geomagnetic cut-off rigidity (COR), averaging over October–November 2006. Symbols are the same as in Figure 6. Lower cut-off rigidity indicates a higher particle background, therefore the narrower line widths at low COR in the FI, charge injection (CI) off data (open points) are due to sacrificial charge. Use of charge injection overwhelms the effects of sacrificial charge, so no dependence on COR is seen in those data (solid points).

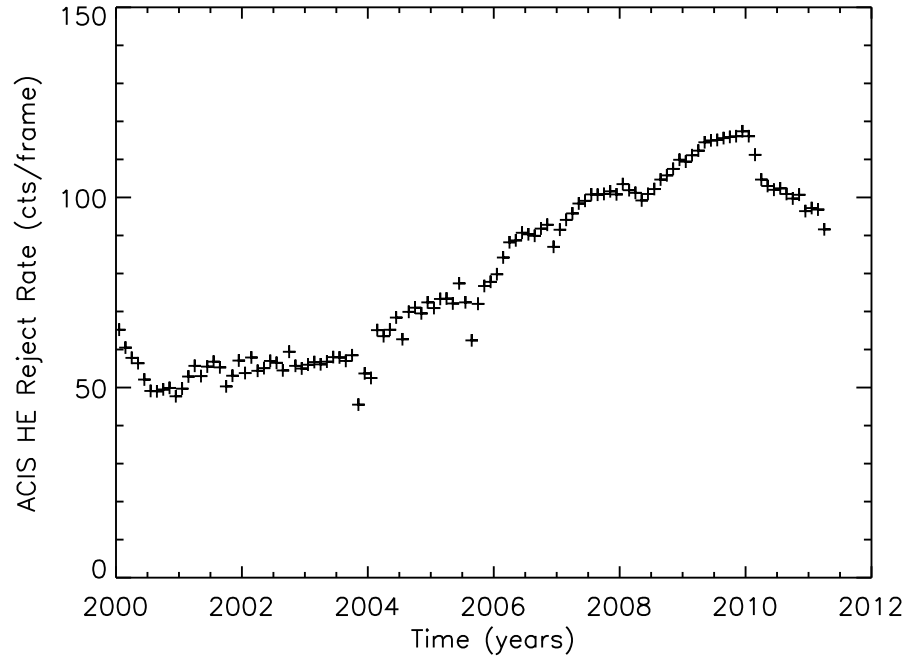


Fig. 11. Time history of the particle background of the *Chandra* mission, measured as the rate of high energy events on ACIS-S3 (BI). The time period and binning are the same as the CTI evolution data. The structure from the varying particle background can be seen in the ACIS line energy data.